




# Smart fabric strain sensor comprising reduced graphene oxide with structure-based negative piezoresistivity

Xinghua Hong<sup>1,2,\*</sup> , Rufang Yu<sup>1</sup>, Min Hou<sup>3</sup>, Zimin Jin<sup>1</sup>, Yubing Dong<sup>3</sup>, Chengyan Zhu<sup>1</sup>, Junmin Wan<sup>2,3</sup>, and Yongqiang Li<sup>1,2</sup>

<sup>1</sup> College of Textiles (International Silk Institute), Key Laboratory of Advanced Textile Materials and Manufacturing Technology, Ministry of Education, Zhejiang Sci-Tech University, Hangzhou 310018, Zhejiang Province, People's Republic of China

<sup>2</sup> Zhejiang Sci-Tech University Tongxiang Research Institute, Tongxiang 314599, Zhejiang Province, People's Republic of China

<sup>3</sup> School of Materials Science and Engineering, Zhejiang Sci-Tech University, Hangzhou 310018, Zhejiang Province, People's Republic of China

Received: 15 March 2021

Accepted: 17 July 2021

Published online:

30 July 2021

© The Author(s), under exclusive licence to Springer Science+Business Media, LLC, part of Springer Nature 2021

## ABSTRACT

Fabric strain sensors have attracted significantly increased interest as wearable electronics for their flexibility, softness, and wearing comfort in recent years. However, most of the fabric strain sensors fail to pay attention to directionality (negative piezoresistivity) and it remains a big challenge to fabricate wearable fabric strain sensors with a broad sensing range. Here, the strain sensing fabric comprising reduced graphene oxide is developed by using a facile dip-dry-reduce method. Compared to the prior textile strain sensors, the remarkable deformation capacity and a broad reversible strain sensing range (up to 450% strain without breaking) of our treated fabric are with special attention. Meanwhile, it owns great sensitivity (gauge factor of -5.92 under 10.7% strain), stability (> 1000 cycles) and reliability. In addition, sensing strain such as tensile, twist, shear and poke is quantitatively determined. Moreover, the sensing fabric exhibits resistance strain anisotropy ( $\Delta R/R_0$  at the wale direction /  $\Delta R/R_0$  at the course direction = 5.23), electric thermal behavior (about 60 °C under a voltage of 10 V). Finally, the equivalent electrical circuit is provided based on the structure, which is presented for the analysis of electromechanical behaviors, structure–activity relationship, transport models and mechanism. Based on this work, the strain sensing fabric comprising reduced graphene oxide can be knitted to shape for application in human motion detection and electric heater as a kind of flexible smart electronic.

Handling Editor: Dale Huber.

Address correspondence to E-mail: xinghuahong@zstu.edu.cn

## Introduction

Wearable strain sensors own many features, including high sensitivity, good flexibility and stretchability, lightweight. There are various types of strain sensors including resistance sensor based on strain effect or piezoresistive effect [1, 2], inductance sensor based on electromagnetic induction [3], Hall sensor based on the Hall effect [4, 5], photoelectric sensor based on the photoelectric effect [6], and piezoelectric sensor based on piezoelectric effect [7–9]. The resistance sensors have received considerable report as they are attractive for use as strain sensor and sign expression [10–13]. Resistance sensor usually requires the material with electrical conductivity. Nevertheless, the inherently conductive fibers (e.g., carbon fiber, metal fiber, and intrinsically conductive polymers) are greatly limited in the application as flexible sensing materials for their brittleness, poor flexibility and weaving-ability. Meanwhile, conventional strain sensors based on metal foils or semiconductors are generally rigid, high weight and have poor stretchability (typically less than 5%), which make them are not true of flexible and wearable strain sensors [14–16].

Fabric strain sensors have attracted considerable attention as wearable electronics recently, mainly because of their friendly compatible with human body [17] and their wide applications such as human motions monitoring [18–22], information gloves [23], speech recognition [24, 25] and entertainment [26]. However, the great majority of fabrics are commonly not electrically conductive. Moreover, the non-conductive fibers or fabrics are most commonly combined with conductive agents, including carbon materials, metal particles and conductive polymers.

Graphene has been extensively adopted to prepare wearable fabric strain sensors due to its outstanding mechanical and electrical properties [20, 24, 26, 27]. Graphene is a two-dimensional carbon nanomaterial [28], which is formed by  $sp^2$  hybridization carbon atoms [29]. Thanks to its electrical conductivity, biocompatibility, excellent thermal and mechanical stability, and strong adhesion with the textile surface via van der Waals interaction (due to its large specific surface area), graphene is considered as a strong candidate material for the high-performance wearable strain sensors [30–34]. On the other hand, textile materials from fiber to yarn and then fabric, all as

flexible materials, own many particular characteristics, such as washability, lightweight, porous structure, high surface area, deformability, sufficient strength and tear resistance [35–38]. Knitted textiles, which are easy to deform due to the unique loop fabric structure, are regarded as an ideal carrier for fabrication of wearable strain sensors [10]. Therefore, more and more researchers effectively combine graphene with knitted fabrics to prepare wearable strain sensors with high sensitivity, good stability and stretchability [10, 13, 17, 32, 35]. Zhang et al. [13] fabricated a wearable graphene textile strain sensor, but a relatively low sensitivity was observed, with a gauge factor (GF) of -1.7 in the strain range of 15% during x-direction stretching. Hanna Lee et al. [10] obtained a strain sensor made from a weft-knit spandex/nylon fabric. The sensor held good sensitivity (high GF of 18.24 within 40.6% strain) and tensile properties. However, the repeatability was seldom provided. Cai et al. [35] manufactured flexible strain sensing fabrics, which displayed high sensitivity (gauge factors of 18.5 and 12.1 under 0–10% and 10–18% strain, respectively) and high stability. Ravinder Reddy K et al. [32] prepared the reduced graphene oxide polyester knitted elastic band strain sensor with high GF of 34 under 0–20% strain. Up to now, most of the wearable strain sensors based on graphene fail to pay attention to directionality (negative piezoresistivity), which may lead to some confusion in data analysis and mechanism. Besides, it remains a big challenge to fabricate wearable fabric strain sensors with a broad sensing range.

This work demonstrates the concept of negative piezoresistivity for alleviating the unclear phenomenon and mechanism mentioned above. The fabric geometrical mode is obtained, and equivalent circuit model related to fiber body and contact interface is developed by building a hybrid fabric consisting of non-conductive fibers and reduced graphene oxide. Therefore, the reduced graphene oxide (RGO) knitted polyester (PET) strain sensing fabric with negative piezoresistivity is fabricated by a low-cost and facile dip-dry-reduce method. Due to conductive networks formed by RGO, the RGO/PET fabric owns an excellent sensitivity with GF of -5.92 under 10.7% strain, good stability (> 1000 cycles, including stretching, poking, shearing and twisting) and reliability. It is worth noting that the RGO/PET fabric holds a broad sensing range (up to 450% applied strain without breaking). In addition, when

the sensing fabric is subjected to tensile strain, poke strain, shear strain and twist strain, it still maintains prominent sensitivity. The RGO/PET strain sensing fabric is successfully used to monitor human motion, such as the bending of fingers, joint movement, and sitting. Furthermore, information gloves made of the sensing fabric can be used to transmit message. More importantly, the RGO/PET fabric is capable of reaching a temperature about 60 °C at a direct current-voltage of 10 V, and about 45 °C at a direct current-voltage of 8 V, which can be controlled by the applied voltage. The RGO/PET fabric without polymer encapsulation has good application potential as strain sensors for wearable electronic devices.

## Experimental section

### Preparation of sensing fabric

Graphene oxide (GO) was obtained by the modified Hummers method (Fig. 1a) [39], as our prior work reported [40], the high concentration reddish-brown of GO dispersion was prepared for standby. The basal fabrics are weft knitted, which are consisting of PET and knitted by using a circular weft knitting machine operating with gauge 40. The wale density and course density of the knitted PET fabric are 200/5 cm and 200/5 cm, respectively. Blended fabrics were cut into small pieces with width by length of  $5 \times 5 \text{ cm}^2$  and treated by using 95% ethyl alcohol and deionized water to remove surface oil, etc. The pre-cleaned fabrics were dipped into high concentrations of GO aqueous solution (pre-ultrasound for 10 min) at room temperature under sonication. Subsequently, the fabrics were dried in an oven at 40 °C. The dip-dry process was repeated 10 cycles. Then, the GO coating fabric was reduced by sufficient amount of hydrazine hydrate and kept for 20 min at 90 °C under closed conditions. The metallic black fabric was obtained. More importantly, RGO is tightly adhered to the surface of fibers mainly thanks to van der Waals interaction and the possible interaction of oxygen-containing functional groups [32, 41]. A good interfacial interaction between the conductive layer and fiber is important for the sensing ability.

### Characterization and measurements

The morphology of graphene fabric was characterized using a SEM (ULTRA-55, JEOL, Japan) with an accelerating voltage of 3.00 kV at room temperature. XRD patterns were recorded using an ARL XTRA diffractometer (USA) in the angular range of  $5\text{--}60^\circ$  ( $2\theta$ ) at a voltage of 40 kV and current of 30 mA. Peak intensities were every  $0.02^\circ$  at sweep rates of  $2.0^\circ 2\theta/\text{min}$ . The mechanical properties of the fabrics were evaluated by an electronic universal material testing machine (EJA SERIES, Thwing-Albert Co., USA). FTIR spectra were used to record the functional groups of samples by using an America FTIR analyzer (Nicolet-5700, USA). The analysis was performed with 64 scans and a spectral range of  $4000\text{--}500 \text{ cm}^{-1}$  for each sample. X-ray photoelectron spectroscopy (XPS) was obtained by using an X-ray photoelectron spectrometer (K-ALPHA, Thermo Fisher Scientific, USA). The resistance change of fabric samples at different strain levels was recorded by using a self-assemble dynamic resistance tester, including resistance meter (SZ2258C, Suzhou Lattice Electronics Co., Ltd., China, and DMM 6500, Tektronix Co. Ltd., China) and abovementioned mechanical test system (EJA SERIES, Thwing-Albert Co., USA).

### Electromechanical analysis

Schematic diagram of electromechanical test system is shown in Fig. 1c. The RGO/PET fabric samples were treated for 24 h at  $23 \pm 1 \text{ }^\circ\text{C}$  and  $50 \pm 2\%$  relative humidity prior to electromechanical measurement. The initial grip separation was set to 28 mm, and all samples were folded into rectangles ( $25 \times 50 \text{ mm}$ ) to fit the tensile grips. The samples were mounted in the fabric-extension grips of the testing machine and stretched at a rate of 1 mm/s, 3 mm/s or 3 mm/step based on the test requirement. Four wood chips with rough surface act as insulation between the conductive grip and fabrics, meanwhile, increasing the friction and holding force (Without the wood chips, the sensing fabric is easy to slip, especially under high elongation strain). The conductive silver paste and aluminum foil are used as two electrodes to connect the fabric and resistance meter.

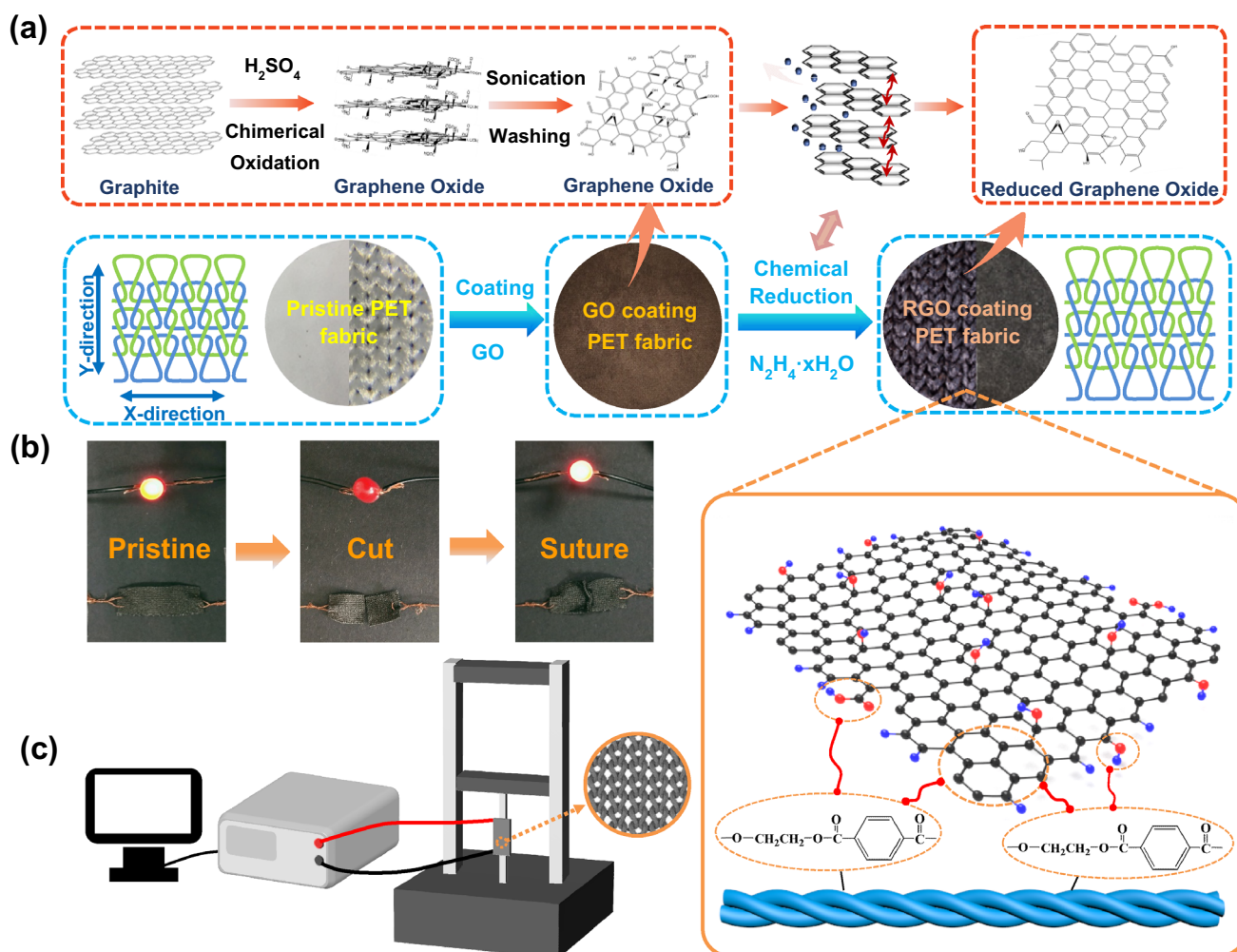


**Figure 1** **a** Illustration showing the structure and preparation process of RGO/PET fabric. **b** Photographs of the RGO/PET fabric connected with a light-emitting diode before and after

cutting and suturing, showing its remarkable electrical conductivity and reparability. **c** Schematic illustration of electromechanical test system.

### Electrothermal analysis

The RGO/PET fabric sample ( $1 \times 2 \text{ cm}^2$ ) was connected with the direct current power supply (E3632A, Agilent, USA) to evaluate its electrothermal performance, while its temperature was recorded by an infrared camera (InfraTec, Germany).

## Results and discussion

### Fabrication and characterization of the RGO/PET fabric

The simple preparation process of RGO/PET fabric is depicted schematically in Fig. 1a. The color of PET fabric changes from white to brown after

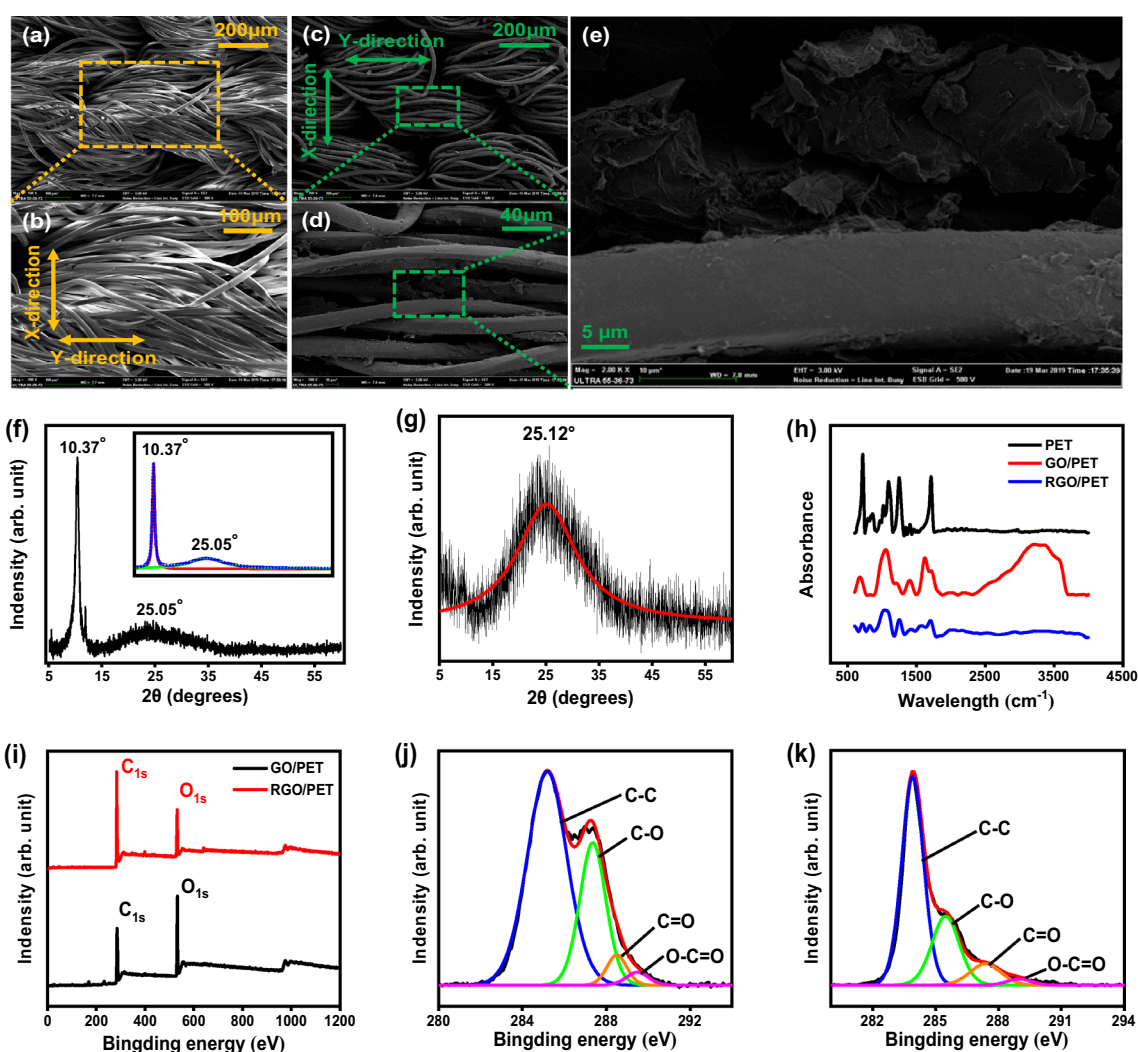
impregnating in GO solution, indicating that GO is adsorbed on the surface of PET fabric. Subsequently, the GO/PET fabric is reduced by hydrazine hydrate, and the color of the reduced fabric changes to light metallic black. The RGO/PET fabric still exhibits an instinctive flexibility like textile materials. The preparation and structural evolution process of layered graphite materials (from graphite to graphite oxide, then reduced graphene oxide) is suspended at the top of Fig. 1a.

Figure 1b shows the reparability of RGO/PET fabric. The photographs of different RGO/PET fabric connected with a light-emitting diode are performed under the same voltage. After the RGO/PET fabric is cut with scissors, it is non-conducting and the diode lights out. Then, the broken fabric is sutured with

common non-conductive yarn. The brightness of the light-emitting diode is almost unchanged before and after suturing, demonstrating the RGO/PET fabric holds remarkable repairability. Suturing can effectively prevent loosening and further damage of the knitting structure. In addition, the resistance of RGO/PET fabric remains almost constant before and after suturing, which is important when the fabric is damaged.

The morphologies, structure and composition of different samples are observed (Fig. 2). Figure 2a and b shows typical scanning electron microscope (SEM)

images of the PET fabric. SEM images of the PET fabric at different magnifications are observed in order to further analyze their morphology. The surface of the original fabric is smooth, without obvious impurities, and the spaces between fibers and tows are about 1–100  $\mu\text{m}$  (Fig. 2b). Figure 2c–e shows the surface of RGO coated PET fabric, which exhibit the flake-like structures and curly edges. As illustrated in Fig. 2e, the vast majority of RGO nanosheets are successfully attached to the surface of PET fabric rather than deposition aggregation between the fibers, and the pore structure of fabric is preserved. In



**Figure 2** Characterizations of the RGO/PET fabric. **a, b** SEM images of the pristine PET fabric under low magnification and high magnification. **c, d** SEM images of the RGO/PET fabric under low magnification and high magnification. **e** Fiber surface morphology of RGO coating PET fabric (high magnification). X-direction is the lengthwise direction, namely the loops interlaced

orientation and weaving direction, makes for greater stretchability. Y-direction is the warp direction. **f, g** XRD spectrum of lyophilized GO particle and RGO particle. **h** FTIR spectra of pristine PET fabric, GO/PET fabric and RGO/PET fabric. **i** XPS spectra of GO/PET fabric and RGO/PET fabric. **j, k**  $\text{C}_{1s}$  spectra of GO/PET fabric and RGO/PET fabric.

addition, a small portion of the RGO nanosheets is stripped from the fibers and deposited in the fibers. Its size can be up to 20  $\mu\text{m}$ , which is close to the diameter of the fiber. The RGO is penetrated evenly into the fabric (ascribed to the multi-void structure), resulting in fabric conductive networks. Thanks to the special structure of the knitted fabrics, these fabric conductive networks can withstand the tensile deformation in different directions, showing excellent mechanical and electrical capacity, as well as anisotropy.

As illustrated in Fig. 2f and g, X-ray diffraction (XRD) is adopted to demonstrate successful preparation and reduction of graphite oxide, pertains to the lattice plane structure of lyophilized GO particle and RGO particle. XRD pattern of lyophilized GO particle in Fig. 2f owns a sharp peak at  $2\theta = 10.37^\circ$ . According to the Bragg Eq. ( $2d\sin\theta = n\lambda$ ), the interlayer spacing can be calculated as 8.52 Å. The interlayer spacing of lyophilized GO particle is larger than that of graphite, which is because of intercalation of functional groups in GO layers. It is worth noting that the lyophilized GO particle also shows another weak shoulder peak at  $25.05^\circ$ , corresponding to an interlayer spacing of 3.55 Å. That is probably due to the residual of some oxygen-containing functional groups by water molecules after freeze-drying, and the incomplete intercalation of a small amount of materials [42]. In addition, it has been reported that the amount of adsorbed moisture affects the interlayer spacing of GO [40]. Moreover, this shoulder peak may be contributed to the partial reduction or impurity as it is close to the main characteristic peak ( $25.12^\circ$ ) of RGO as shown in Fig. 2g. The broadened diffraction peak at  $25.12^\circ$  is found in the XRD pattern of RGO particle (Fig. 2g), which corresponds to an interlayer spacing of 3.54 Å. It indicates that the crystallinity of RGO is not perfect as the raw graphite. The RGO still remains a small number of oxygen-containing functional groups [43] and defect.

FTIR spectrums of pristine PET fabric, GO/PET fabric and RGO/PET fabric are demonstrated in Fig. 2h. In the FTIR spectrum of pristine PET fabric, the characteristic peaks appear at 716, 858, 1093, 1247 and 1710  $\text{cm}^{-1}$ , which are attributed to the bending vibration of -CH, trans conformations of oxy-ethylene groups, O-C-O stretching, asymmetric stretch C-C-O group bonded to aromatic ring, stretching vibrations of C=O, respectively [44–46]. When the fabric dips into GO solution, the FTIR spectrum of GO/PET

fabric is closed to the typical FTIR spectrum of GO [47], which indicates the efficient coating of GO. Compared to the pristine PET fabric, a prominent peak around 2335–3700  $\text{cm}^{-1}$  appears due to the stretching vibration of O-H and the strong interaction between the high content of adsorbed water [48, 49]. The slight shift and weakening of characteristic peaks are associated with the oxygen-containing functional groups of GO, showing an interaction between PET fabric and GO. After hydrazine hydrate reduction, the wide peaks at 2335–3700  $\text{cm}^{-1}$  disappears, indicating the reduction significantly and removal of oxygen-containing functional groups.

XPS is employed to further confirm the reduction of GO and analyze the composition of the fabric. Figure 2i displays XPS spectra of GO/PET fabric and RGO/PET fabric. It can be observed that the  $\text{C}_{1s}$  and  $\text{O}_{1s}$  peaks appear at 284 and 533 eV, respectively. The C/O ratios of GO/PET fabric and RGO/PET fabric are 0.98 and 1.67, respectively. As illustrated in  $\text{C}_{1s}$  spectra of GO/PET fabric and RGO/PET fabric (Fig. 2j, k), there are four peaks locate at 284.2, 285.7, 287.5, and 288.6 eV, corresponding to C-C, C-O, C=O and O-C=O [50]. Both the change in peak intensities of RGO/PET fabric in  $\text{C}_{1s}$  spectra and the increase of C/O ratio testify that GO is reduced.

### Electromechanical behaviors of the RGO/PET fabric

The electromechanical properties of RGO/PET fabric are crucial to their applications. The electrical conductivity of the RGO/PET fabric is 430.94 mS/cm. After two standard washing cycles, the electrical conductivity drops by 59%. This is mainly caused by the stripping of the RGO nanosheets deposited in the fibers. The RGO/PET sensing fabric exhibits high sensitivity and negative piezoresistivity under the strain. As illustrated in Fig. 3a, the RGO/PET fabric possesses a negative resistance variation ( $\Delta R/R_0$ ) under cyclic tensile strain include wale and course direction, where  $R_0$  represents the initial resistance, and  $\Delta R$  represents the difference between real-time resistance (R) and the initial resistance ( $R_0$ ). The negative piezoresistivity is a kind of structure-based negative piezoresistivity (SNP), refer to the direction vector rather than negative electrons, etc. The RGO/PET fabric exhibits outstanding durability and stability in wale and course direction during 240

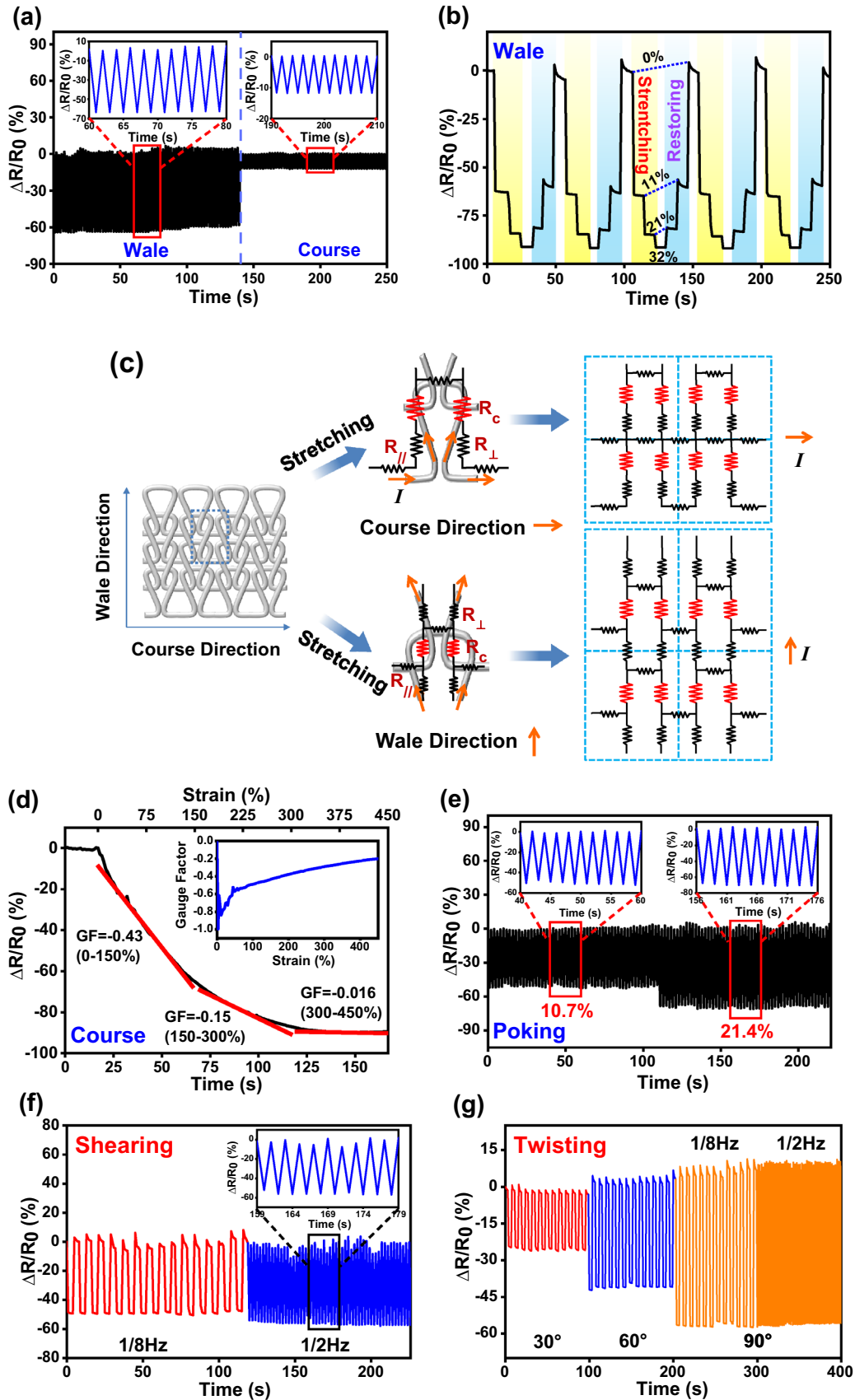


**Figure 3** Electromechanical characterization of the RGO/PET fabric. **a** Relative resistance variation versus cyclic tensile strain of 10.7% include wale and course direction (durability test for 240 times). **b** Relative resistance variation versus different cyclic tensile strains of 10.7%, 21.4%, 32.1% (wale direction). **c** Schematic diagram of the resistance strain anisotropy. Equivalent circuit models in course and wale directions ( $R_c$  represents the contact resistance,  $R_{//}$  represents the resistance of the course direction,  $R_{\perp}$  represents the resistance of the wale direction). **d** Relative resistance changes ( $\Delta R/R_0$ ) of the RGO/PET fabric versus the applied tensile strain (course direction). **e** Relative resistance variation of the RGO/PET fabric under cyclic stretching-releasing when it is poked with strain of 10.7% and 21.4%. **f** Relative change in resistance versus time under cyclic shearing strain at frequencies of 1/8 and 1/2 Hz. **g** Relative resistance change of the RGO/PET fabric versus cyclic stretching-releasing at twisting angles of 30°, 60° and 90°.

cycles of 10.7% strain. The resistance variation of RGO/PET fabric in wale and course direction is significantly different. When the tensile strain is applied in the wale direction with 10.7% strain, the resistance decreases by  $\sim 63\%$ , while the resistance in the course direction decreases by  $\sim 12\%$  in the same strain. Therefore, the wale/course resistance variation ratio is  $\sim 5.2$  corresponding to the resistance strain anisotropy. The RGO/PET fabric holds anisotropic strain sensing features, which cannot be obtained by isotropic fabrics such as woven fabrics.

It is worth noting that the resistance strain anisotropy exists in each deformation stage, and its orientation can be determined according to the resistance strain anisotropy when the strain is known. To explain the resistance strain anisotropy when the RGO/PET fabric is stretched, equivalent circuit models in course and wale directions are depicted in Fig. 3c. Current is able to pass from one loop to the next both in wale and course direction. Based on this, equivalent circuit models of the RGO/PET fabric are established according to these unit loops in wale and course direction, respectively.  $R_c$  represents the contact resistance,  $R_{//}$  represents the resistance of the course direction,  $R_{\perp}$  represents the resistance of the wale direction. In course direction, the current passes through  $R_{//}$ ,  $R_{\perp}$ ,  $R_c$ ,  $R_{//}$ ,  $R_c$ ,  $R_{//}$  and  $R_{\perp}$ , respectively. In wale direction, the current mainly passes through  $R_{\perp}$ ,  $R_c$  and  $R_{//}$ . Meanwhile, a small amount of current passes through  $R_{//}$ . It can be found that equivalent circuit networks of wale and course direction are different, which leads to the

resistance strain anisotropy. All in all, the model takes account of fabric loop structure and current conduction directivity.

In order to test the reliability of the RGO/PET fabric, relative resistance variation of the RGO/PET fabric under different cyclic tensile strain of 10.7%, 21.4%, 32.1% in the wale direction is demonstrated in Fig. 3b. It can be seen that the RGO/PET fabric is sensitive to different tensile strain and  $\Delta R/R_0$  changes steadily with repeatability. The relative value of  $\Delta R/R_0$  decreases by  $\sim 90\%$  under 32% tensile strain. The signal remains stable in each cycle without significant drifts, showing the sensing fabric possesses excellent performance in terms of sensitivity.

Figure 3d displays a typical curve of relative resistance variation of the RGO/PET fabric with tensile strain in the course direction. There is a non-linear relationship between relative resistance variation and strain when the RGO/PET fabric is stretched up to 450%. And the maximum stretch of 450% only happens in the course direction. In addition, in the strain range of 0–450%, the RGO/PET fabric owns GFs within range of -0.2 to -1.0. With the increase of strain, the relative resistance shows a negative resistance variation and changes monotonically decrease. It can be found that the RGO/PET fabric owns GFs of -0.43, -0.15 and -0.016 under 0–150%, 150–300% and 300–450% strain, respectively. It indicates the sensitivity of fabric decreases with increment of tensile strain. Although the GF of RGO/PET fabric drops to -0.016 when the strain is 300%  $\sim$  450%, its resistance still changes and the variation of strain can be sensed. This is mainly contributed to the contact between the fibers and the loops become very close and tight with the increase of strain. Therefore, the change of the conductive networks composed of these contacts gradually decreases and even tends to be stable. This also reflects that the RGO/PET fabric can be stretched to 450% without breaking. If the RGO/PET fabric is broken, destruction and reconstruction of conductive networks attached to the fiber surface will play a leading role, which will lead to the increase of its resistance. To sum up, the RGO/PET fabric has excellent deformation capacity and a wide reversible strain sensing range at least up to 450% without breaking.

The RGO/PET fabric will be subjected to various external forces in practical application. Therefore, besides stretching, the effects of poking, shearing and twisting on the resistance of RGO/PET fabric are also



investigated. Figure 3e shows the typical curve of relative resistance change of the RGO/PET fabric when it is poked with different strain ( $\sim 10.7\%$ ,  $\sim 21.4\%$ ). The relative resistance variation  $\Delta R/R_0$  of the RGO/PET fabric decreases by  $\sim 50\%$  when poked with strain of  $10.7\%$ , while that decreases by  $\sim 70\%$  under a poking strain of  $21.4\%$ . It can be found that the fabric is successful in sensing different degrees of poking strain. Furthermore, the curve indicates that the signal remains stable when the same strain is poked to the RGO/PET fabric.

When shearing strain is applied to the RGO/PET fabric, its relative resistance variation is demonstrated in Fig. 3f. The applied shearing refers to one side of the fabric sample is secured, and the other side is given horizontal movement. The influence of a strain frequency on the fabric sensing properties is studied. It can be seen that the relative resistance of the RGO/PET fabric decreases by  $\sim 50\%$  and hardly changes at the measured frequencies of  $0.125$  Hz and  $0.5$  Hz, demonstrating the relative changes in resistance  $\Delta R/R_0$  of the sensing fabric have no dependence on the applied strain frequency. Moreover, the relative variation of resistance keeps stable at each frequency.

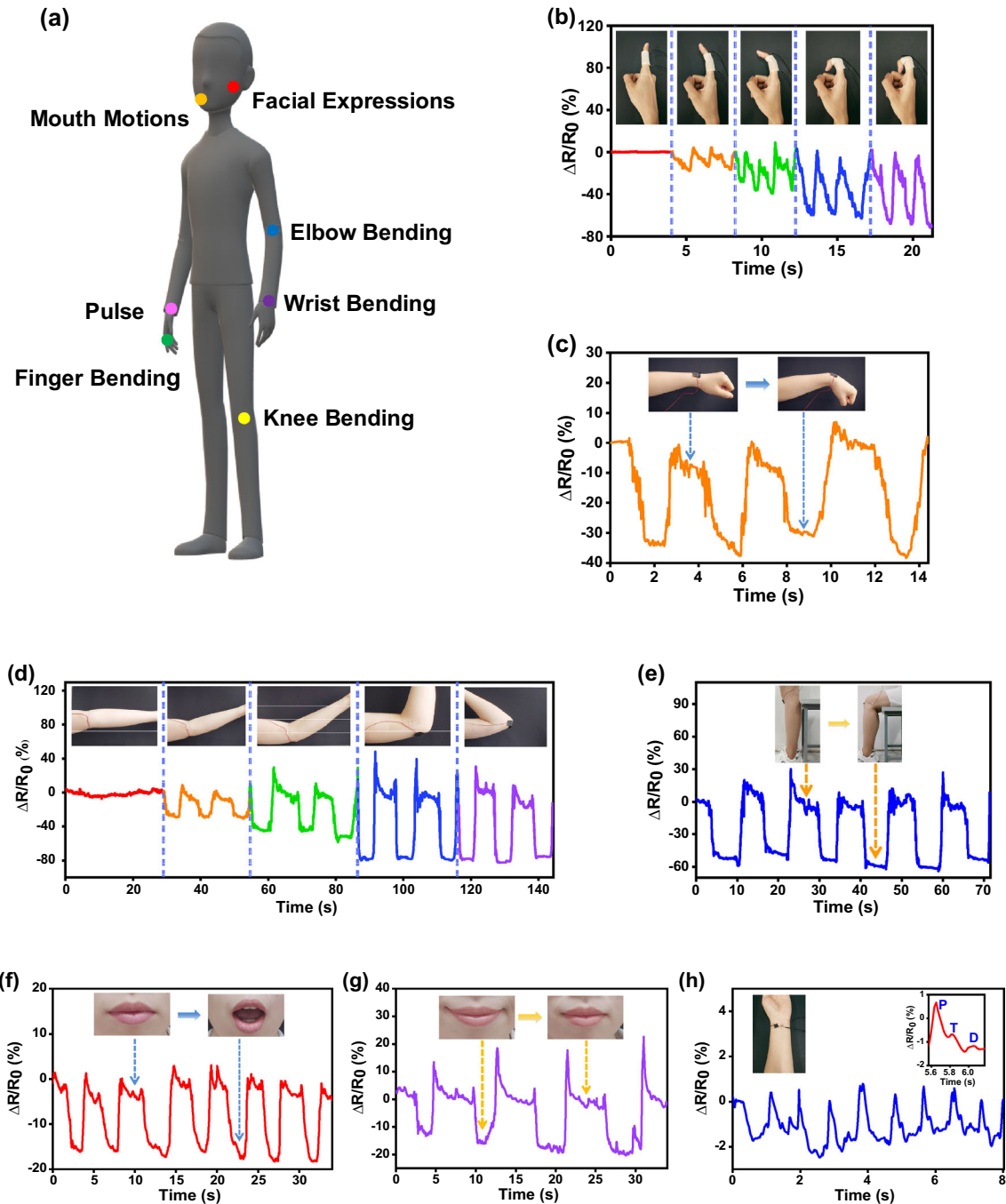
In order to further study the dynamic response of the RGO/PET fabric, the effect of twist angle on the sensing performance is also performed. Figure 3g presents the change of relative resistance at twist angle of  $30^\circ$ ,  $60^\circ$  and  $90^\circ$ . The sensing fabric holds remarkable sensitivity to the twist angle and outstanding stability. The value of  $\Delta R/R_0$  decreases by  $\sim 25\%$  when it is twisted by  $30^\circ$  and decreases by  $\sim 43\%$  when it is twisted by  $60^\circ$ , while that decreases by  $\sim 60\%$  when it is twisted by  $90^\circ$ . With the increase of the twist angle, the amplitude of relative change in resistance  $\Delta R/R_0$  of the RGO/PET fabric increases. The reason may be the torsion deformation of fabric causes the loop structure change to close and tight, and then the conductive RGO nanosheets attached to the fiber surface have more electrical contact. Furthermore, when the RGO/PET fabric is twisted by  $90^\circ$ , the influence of torsion frequency on the resistance signal of RGO/PET fabric is also tested. It can be seen that the change of relative resistance is independent of frequency. The value of  $\Delta R/R_0$  is always stable when the RGO/PET fabric is twisted by  $90^\circ$ .

Table S1 (in the Supporting Information) shows performances of various recently reported fabric

strain sensors. Readers can search for the information listed in Table S1 to find materials with the best GF or other advantages. It is worth noting that the RGO/PET fabric owns extra-high stretchability (up to  $450\%$ ). This is determined by the structural characteristics of the fabric rather than the fiber is stretched by  $450\%$ . It is known that the stretchability of RGO is quite poor, because the RGO is physical adhere on the surface of fabric. However, in this paper, the RGO can well preserve its structure stability after such large range stretch (up to  $450\%$ ). In addition, stability is an important factor to evaluate the performance of sensing materials. In this paper, the stability of RGO/PET fabric under various strain behaviors (includes tensile strain, twist strain, shear strain and poke strain) is studied. It can be found that the RGO/PET fabric holds prominent stability after more than 1000 cycles of different strain. It is important to note that more than 1000 cycles refer to the total number of various strain cycles. In general, the RGO/PET fabric possesses prominent electrical performance including high sensitivity, excellent stability and stretchability. These remarkable features endow them great potential for applications in the future of wearable electronics.

### Applications of the RGO/PET fabric

To demonstrate the potential applications of the RGO/PET fabric, the fabric is mounted on different joints for monitoring human motions (Fig. 4a). As illustrated in Fig. 4b, the RGO/PET fabric is attached on a finger to detect movement. The relative resistance variation  $\Delta R/R_0$  remains stable when the finger bends to a certain angle. The amplitude of relative resistance variation increases with the increase of bending angle. What is more, detecting the relative resistance variation can accurately track the angle of the finger bending. In Fig. 4c, the RGO/PET fabric is affixed on the wrist joint for sensing wrist bending and recovering. When the wrist joint bend to a certain angle, the relative value of  $\Delta R/R_0$  decreases and keep stable. Then, the relative resistance returns to initial state after the wrist recover. As shown in Fig. 4d, the sensing fabric also succeeds in monitoring elbow motions, demonstrating the repeatable resistance variation signal. In order to monitor movement of the knee, the RGO/PET fabric is mounted on the knee joint (Fig. 4e). It can be found that the fabric successfully detects standing and sitting behavior of



**Figure 4** The RGO/PET sensing fabric for various human motion detection. **a** Schematic illustration of the fabric mounted on different joints for monitoring human motions. **b** Detection of different finger bending angles. **c** The responses to human motions of wrist bend. **d** Relative change in resistance of the elbow joint bending with different angles. **e** Corresponding signals of the

bending of a knee joint. **f** Monitoring of the mouth motions of opening and closing. **g** Responsive curves of the RGO/PET fabric to laughing. **h** Signal of pulse. The suspending curve shows three characteristic peaks that corresponding to P-wave, T-wave and D-wave.

human. In addition to monitoring large motions, the RGO/PET fabric can also detect subtle human motions, including mouth motion, facial expressions

and pulse. Figure 4f presents the relative resistance variation when the mouth opens and closes. The RGO/PET sensing fabric can also be employed for

the real-time monitor of facial expressions as Fig. 4g shown. What is more, three characteristic peaks that corresponding to the percussion wave (P-wave), tidal wave (T-wave) and diastolic wave (D-wave) are successfully observed in Fig. 4h, showing that the RGO/PET fabric can detect subtle physiological signal and holds prominent sensitivity.

In addition, the RGO/PET fabric can be sewn onto gloves to make information gloves (Fig. 5a). Information gloves are combined with Moss codes to transmit information. The short signal is set to 5 s, while the long signal to 10 s (the interval can be adjusted according to proficiency and sensitivity). Figure 5b–e shows the relative resistance variation of transmit different English letters information, such as “Z,” “S,” “T,” and “U.” By patterning RGO/PET fabric with glove structures, a novel wearable system is created for effective information transfer even during cold, dangerous, and other conditions requiring protective gloves. The above results imply the RGO/PET fabric can successfully detect both subtle and large human motions, and owns a tremendous application prospect as a strain sensor.

### Thermal properties of the RGO/PET fabric

When the RGO/PET fabric is stretched, the resulting deformation is output through an electrical signal, which inevitably produces a certain amount of heat. In addition, carbon-based materials hold remarkable thermal property. Therefore, thermal properties of the RGO/PET fabric are studied. The RGO/PET fabric is put on the back of hand, and an IR camera is adopted to record the evolution of temperature. It can be clearly observed that the temperature of the fabric rises rapidly within 20 s, indicating that the RGO/PET fabric owns good thermal conductivity (Fig. 6a, b). To further evaluate Joule heating performance of the RGO/PET fabric, a wearable RGO/PET fabric heater is fabricated, shown in Fig. 6c. Figure 6d illustrates the variation of average temperature of the RGO/PET fabric under direct current-voltages from 4 to 10 V. The temperature images captured by an infrared camera at each applied voltage are presented in the inset of Fig. 6d. The temperature of the fabric increases gradually when the applied voltage increases. It can be observed that the RGO/PET fabric

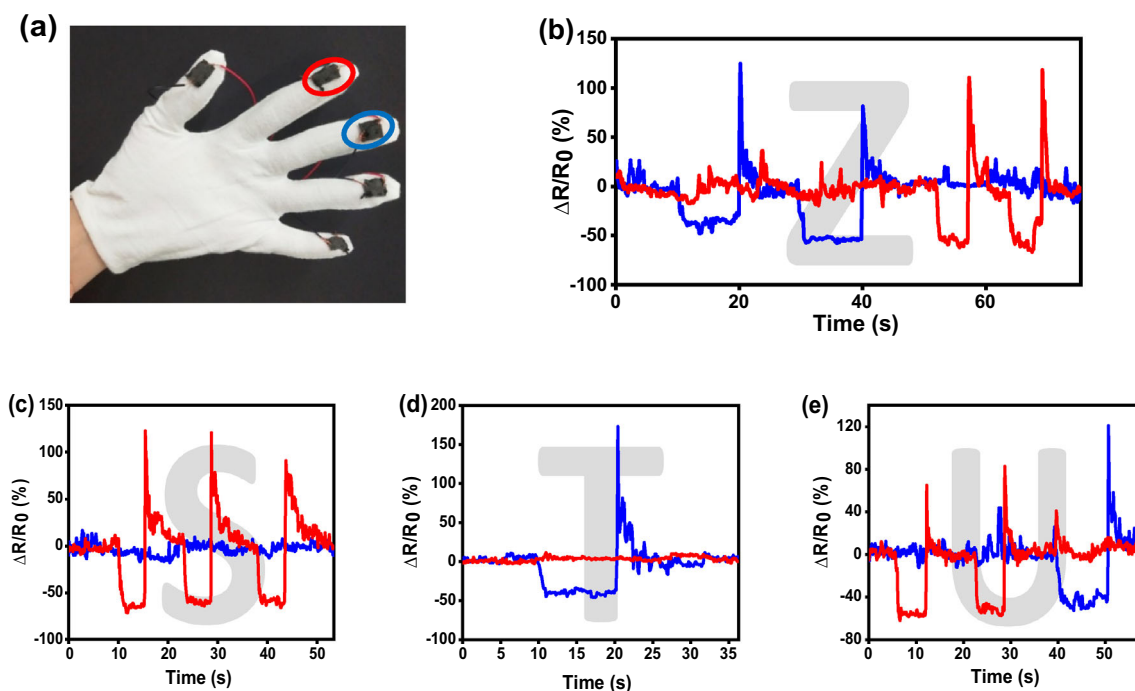


**Figure 5** Applications of information gloves based on the RGO/PET fabric. **a** Schematic diagram of information gloves. **b–e** Schematic diagram of different English letter messages (Z, S, T, U)

transmission by glove, which is corresponding to the relative resistance variation and frequency of a two-finger signal.

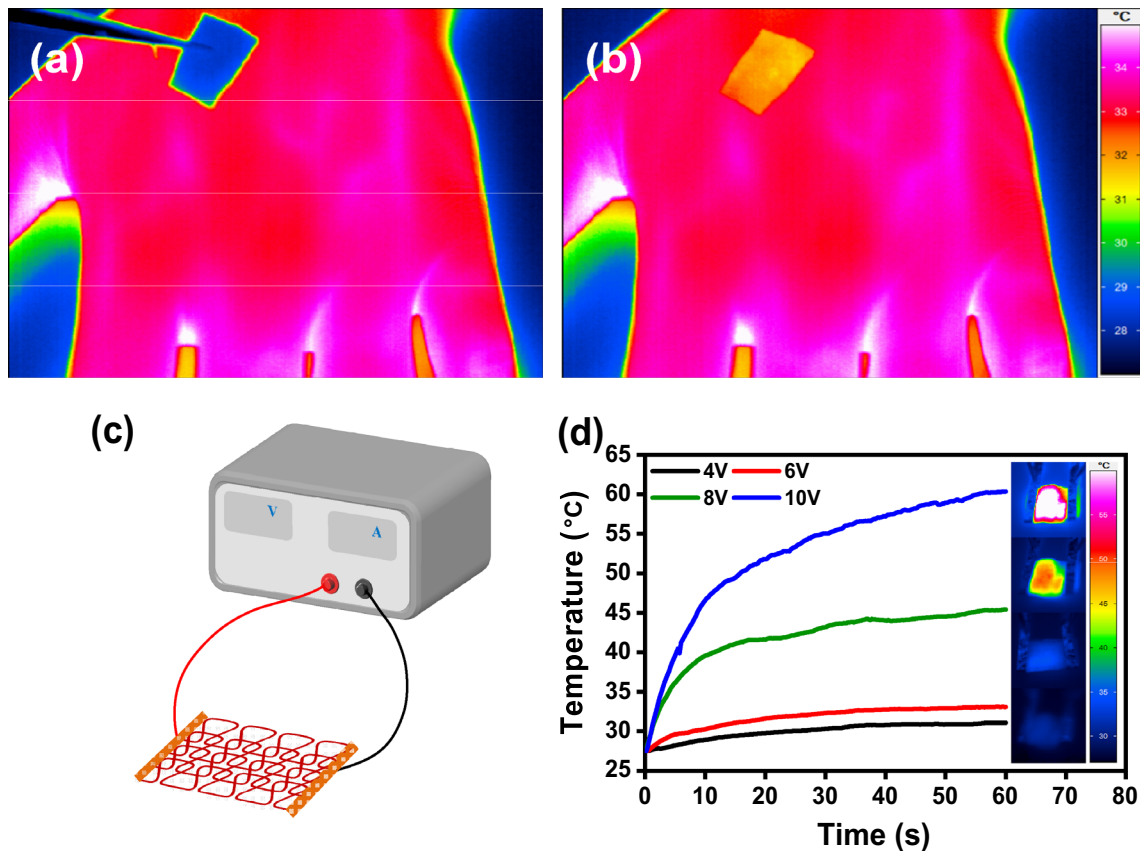


**Figure 6** Thermal behavior of the RGO/PET fabric as a wearable heater. **a, b** Infrared images of the temperature change for the RGO/PET fabric on the hand after about 20 s. **c** Schematic illustration of the wearable RGO/PET fabric. **d** Evolution of the

can reach a temperature about 60 °C, 45 °C, 33 °C, and 31 °C at a direct current-voltage of 10 V, 8 V, 6 V, and 4 V, respectively. What is more, the temperature of the fabric remains stable after reaching a certain value, so that the temperature can be regulated by voltage control and the RGO/PET fabric can be applied as electrical direct heater (EDH).

### Mechanism

The weft-knitted structure of RGO/PET fabric provides an insight into the analysis of mechanisms for electromechanical behavior mentioned above, including the conductivity, deformation and structure–activity relationship. The conductivity is mostly related to the contacts between adjacent fibers, as well as the linear continuity of each fiber. The multilevel contact mechanism is dominant, especially for the electromechanical behavior. A simple resistance model of the RGO/PET strain sensing fabric is

average temperature of the RGO/PET fabric under direct current-voltages from 4 to 10 V. Inset of **d** show temperature images captured by an infrared camera at each applied voltage at 60 s of applying the voltages.

presented in Fig. 7a. In the initial status, RGO is deposited on the surface of fibers and endows the PET fabric with electrical conductivity, so as to form a conductive network. Figure 7b demonstrates shape change process of a PET yarn corresponding to virgin buckling configuration without tension and stretching configuration under tension. It can be clearly seen that a PET yarn consists of many fibers. In the weft-knitted structure, adjacent fibers are in contact with each other, resulting in a large amount of contact between the RGO sheets coated on the fibers, so as to form contact points and conductive networks. In the state of no strain, there is a small gap between fibers. When strain is applied, the fibers on the same yarn become closer, resulting in an increase in the number of contact points between fibers. The existence and slide of contact points not only ensure conductive pathways and a large deformation of knitted structure, but also ensure integrity of the yarn and prevent the fracture in use. More importantly, when the

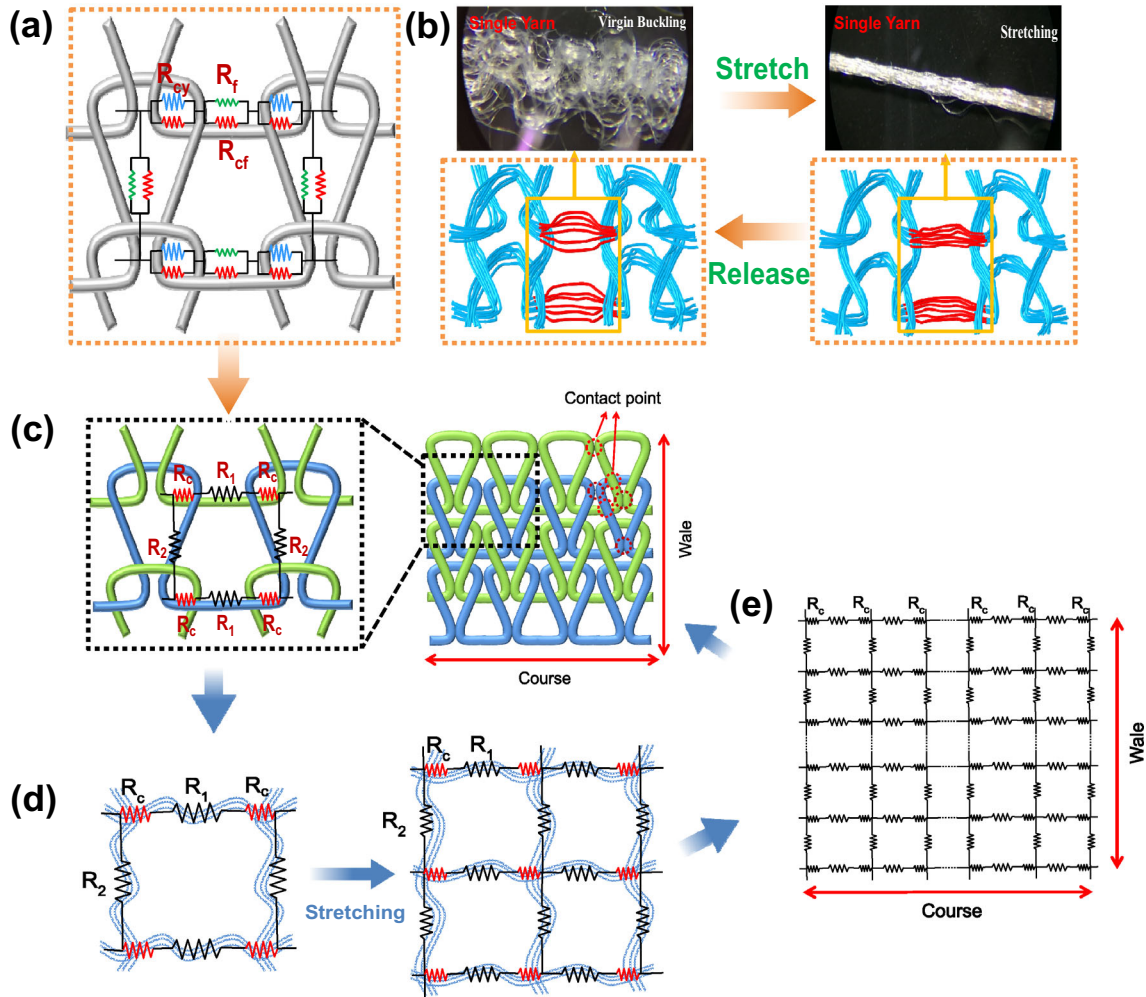


**Figure 7** Sensing mechanism of the RGO/PET fabric. **a** Schematic illustration of a basic unit of the conductive network of the RGO/PET fabric ( $R_f$  represents the resistances of fibers,  $R_{cf}$  represents the contact resistance between fibers,  $R_{cy}$  represents the contact resistance between yarns). **b** Shape change process of a PET yarn and photographs corresponding to virgin buckling configuration without tension and stretching

configuration under tension. **c** Schematic illustration of a basic unit of the conductive network of the RGO/PET fabric without considering the contact resistance between fibers. **d** Evolution of the conductive network structural of the RGO/PET fabric under strain. **e** Schematic illustration of the simple model of the conductive networks of the RGO/PET fabric.

RGO/PET fabric is subjected to strain, the quantity of contact points and the conductive pathways are increased, leading to the resistance decreases (change in reverse with the strain), demonstrating the negative piezoresistivity.

In order to deeply understand the relationship between the fabric structure and the relative resistance variation, the resistance model is simplified without considering the contact resistance between fibers (Fig. 7c–e). As shown in Fig. 7c, an elementary unit can be divided into two parts ( $R_c + R_1 + R_c + R_2$  and  $R_2 + R_c + R_1 + R_c$ ). It can be regarded as

a parallel circuit. Therefore, the total resistance ( $R_t$ ) of the elementary unit can be demonstrated using the following equation

$$R_t = \frac{R_1 + R_2 + 2R_c}{2} \tag{1}$$

where  $R_1$  and  $R_2$  are the resistances of the longitudinal yarn and the transverse yarn in an elementary unit without any applied strain, respectively.  $R_c$  is the contact resistance when no strain is applied. In the state of no strain, thanks to the unique weft-knitted structure of the RGO/PET fabric, the longitudinal yarn and the transverse yarn are in contact

with each other and there is a small gap between fibers. This results in a very high value of  $R_c$ . The resistance  $R_1$  and  $R_2$  are so small that can be neglected compared to  $R_c$ . As a result, the total resistance can be approximated to the contact resistance.

Figure 7d presents a simple diagram of the evolution of the conductive network structure under stretching. When the strain is applied, the fibers on the same yarn become tighter. It results in a decrease in the resistance of the longitudinal yarn and the transverse yarn. At the same time, the number of contact points between fibers increases accordingly with increasing strain, thus leading to the variation of the contact resistance. The contact resistance can be represented by the Holm's contact theory [51].

$$R_c = \frac{\rho}{2} \sqrt{\frac{\pi H}{nP}} \quad (2)$$

where  $\rho$  is the electrical resistivity,  $H$  is the hardness,  $n$  is the number of contact points and  $P$  is the contact pressure. Equation 2 shows that  $R_c$  will decrease with increasing the number of contact points and the contact pressure (assuming the electrical resistivity and hardness remain unchanged). Therefore,  $R_1$ ,  $R_2$  and  $R_c$  all decrease and the resistance of the RGO/PET fabric under strain is less than the initial resistance  $R_i$ . In addition, the number of conductive pathways increases with the increase of contact points during the stretching process, which also leads to a decrease in the total resistance. This indicates the negative resistance variation of the RGO/PET fabric. To sum up, the above models reasonably interpret the relationship between the structural deformation of the RGO/PET fabric and the variation of relative resistance.

## Conclusions

In summary, we have fabricated a smart strain sensing fabric with SNP via a facile and safe dip-dry-reduce method. The RGO/PET fabric is endowed with high sensitivity (a GF of -5.92 under a strain of 10.7%), broad sensing range (up to 450% applied strain), remarkable long-term durability and stability, and exhibits resistance strain anisotropy ( $\Delta R/R_0$  at the wale direction /  $\Delta R/R_0$  at the course direction = 5.23). The sensing fabric succeeds in monitoring various human motions in real-time, including the bending of fingers, joint movement, pulse, etc. In

addition, the RGO/PET fabric can reach a temperature about 60 °C, 45 °C, 33 °C, and 31 °C at a direct current-voltage of 10 V, 8 V, 6 V, and 4 V, respectively. The temperature of the fabric can be controlled by the applied voltage and remains stable after reaching a certain value. Moreover, equivalent electrical circuit is provided based on the structure (include conductivity, contact resistance, deformation), which is presented for the analysis of electromechanical behaviors, structure–activity relationship, transport models and mechanism. Based on this work and its superior performance, the RGO/PET fabric, as a kind of wearable strain sensing fabric and flexible electronic, can be knitted to shape and has tremendous potential for applications in human motion capture and detection, EDH, and information transmit.

## Acknowledgements

This research was supported by the National Natural Science Foundation of China (NSFC 51803185), Public Welfare Project of Zhejiang Province (LGF21E030005), China Postdoctoral Science Foundation (2020M681917), Postdoctoral Foundation of Zhejiang Sci-Tech University Tongxiang Research Institute (TYY202013), the Science Foundation of Zhejiang Sci-Tech University (No. 18012107-Y).

**Supplementary Information:** The online version contains supplementary material available at <http://doi.org/10.1007/s10853-021-06365-4>.

## References

- [1] Jia Y, Yue X, Wang Y, Yan C, Zheng G, Dai K, Liu C, Shen C (2020) Multifunctional stretchable strain sensor based on polydopamine/ reduced graphene oxide/ electrospun thermoplastic polyurethane fibrous mats for human motion detection and environment monitoring. *Compos B Eng* 183:107696. <https://doi.org/10.1016/j.compositesb.2019.107696>
- [2] Yi F-L, Meng F-C, Li Y-Q, Huang P, Hu N, Liao K, Fu S-Y (2020) Highly stretchable CNT Fiber/PAAm hydrogel composite simultaneously serving as strain sensor and supercapacitor. *Compos B Eng* 198:108246. <https://doi.org/10.1016/j.compositesb.2020.108246>

- [3] Matsuzaki R, Todoroki A, Kobayashi H, Shimamura Y (2005) Passive wireless strain monitoring of a tire using capacitance and electromagnetic induction change. *Adv Compos Mater* 14(2):147–164. <https://doi.org/10.1163/1568551053970663>
- [4] Ozer B, Piskin H, Akdogan N (2019) Shapeable planar hall sensor with a stable sensitivity under concave and convex bending. *IEEE Sens J* 19(14):5493–5498. <https://doi.org/10.1109/JSEN.2019.2907616>
- [5] Nguyen T-K, Phan H-P, Han J, Dinh T, Mdfoisal AR, Zhu Y, Nguyen N-T, Dao DV (2018) Utilizing large hall offset voltage for conversion free 4H-SiC strain sensor. In: *IEEE Micro Electro Mechanical Systems*, pp 882–885. <https://doi.org/10.1109/MEMSYS.2018.8346697>
- [6] Eom J-H, Choi H-J, Pammi SVN, Tran V-D, Kim Y-J, Kim H-J, Yoon S-G (2018) Self-powered pressure and light sensitive bimodal sensors based on long-term stable piezoelectric MAPbI<sub>3</sub> thin films. *Journal of Materials Chemistry C* 6(11):2786–2792. <https://doi.org/10.1039/c8tc00081f>
- [7] Huo Z, Wang X, Zhang Y, Wan B, Wu W, Xi J, Yang Z, Hu G, Li X, Pan C (2020) High-performance Sb-doped p-ZnO NW films for self-powered piezoelectric strain sensors. *Nano Energy* 73:104744. <https://doi.org/10.1016/j.nanoen.2020.104744>
- [8] Koziół M, Toroń B, Szperlich P, Jesionek M (2019) Fabrication of a piezoelectric strain sensor based on SbSI nanowires as a structural element of a FRP laminate. *Compos B Eng* 157:58–65. <https://doi.org/10.1016/j.compositesb.2018.08.105>
- [9] Yu R, Zhu C, Wan J, Li Y, Hong X (2021) Review of graphene-based textile strain sensors with emphasis on structure activity relationship. *Polymers*. <https://doi.org/10.3390/polym13010151>
- [10] Lee S, Kim M-O, Kang T, Park J, Choi Y (2018) Knit band sensor for myoelectric control of surface emg-based prosthetic hand. *IEEE Sens J* 18(20):8578–8586. <https://doi.org/10.1109/JSEN.2018.2865623>
- [11] Qian Q, Wang Y, Zhang M, Chen L, Feng J, Wang Y, Zhou Y (2019) Ultrasensitive paper-based polyaniline/graphene composite strain sensor for sign language expression. *Compos Sci Technol* 181:107660. <https://doi.org/10.1016/j.compscitech.2019.05.017>
- [12] Costa P, Nunes-Pereira J, Oliveira J, Silva J, Moreira JA, Carabineiro SAC, Buijnsters JG, Lanceros-Mendez S (2017) High-performance graphene-based carbon nanofiller/polymer composites for piezoresistive sensor applications. *Compos Sci Technol* 153:241–252. <https://doi.org/10.1016/j.compscitech.2017.11.001>
- [13] Yang Z, Pang Y, Han XL, Yang Y, Ling J, Jian M, Zhang Y, Yang Y, Ren TL (2018) Graphene textile strain sensor with negative resistance variation for human motion detection. *ACS Nano* 12(9):9134–9141. <https://doi.org/10.1021/acsnano.8b03391>
- [14] Zahid M, Papadopoulou EL, Athanassiou A, Bayer IS (2017) Strain-responsive mercerized conductive cotton fabrics based on PEDOT:PSS/graphene. *Mater Des* 135:213–222. <https://doi.org/10.1016/j.matdes.2017.09.026>
- [15] Huang Y, Gao L, Zhao Y, Guo X, Liu C, Liu P (2017) Highly flexible fabric strain sensor based on graphene nanoplatelet-polyaniline nanocomposites for human gesture recognition. *J Appl Polym Sci* 134(39):45340. <https://doi.org/10.1002/app.45340>
- [16] Zhang M, Wang C, Wang Q, Jian M, Zhang Y (2016) Sheath-core graphite/silk fiber made by dry-meyer-rod-coating for wearable strain sensors. *ACS Appl Mater Interfaces* 8(32):20894–20899. <https://doi.org/10.1021/acsam.6b06984>
- [17] Tian M, Zhao R, Qu L, Chen Z, Chen S, Zhu S, Song W, Zhang X, Sun Y, Fu R (2019) Stretchable and designable textile pattern strain sensors based on graphene decorated conductive nylon filaments. *Macromol Mater Eng* 304(10):1900244. <https://doi.org/10.1002/mame.201900244>
- [18] Wang S, Ning H, Hu N, Liu Y, Liu F, Zou R, Huang K, Wu X, Weng S, Alamusi, (2019) Environmentally-friendly and multifunctional graphene-silk fabric strain sensor for human-motion detection. *Adv Mater Interfaces* 7(1):1901507. <https://doi.org/10.1002/admi.201901507>
- [19] Jiang X, Ren Z, Fu Y, Liu Y, Zou R, Ji G, Ning H, Li Y, Wen J, Qi HJ, Xu C, Fu S, Qiu J, Hu N (2019) Highly compressible and sensitive pressure sensor under large strain based on 3D porous reduced graphene oxide fiber fabrics in wide compression strains. *ACS Appl Mater Interfaces* 11(40):37051–37059. <https://doi.org/10.1021/acsam.9b11596>
- [20] Du D, Li P, Ouyang J (2016) Graphene coated nonwoven fabrics as wearable sensors. *J Mater Chem C* 4(15):3224–3230. <https://doi.org/10.1039/c6tc00350h>
- [21] Liu X, Liu D, Lee JH, Zheng Q, Du X, Zhang X, Xu H, Wang Z, Wu Y, Shen X, Cui J, Mai YW, Kim JK (2019) Spider-web-inspired stretchable graphene woven fabric for highly sensitive, transparent, wearable strain sensors. *ACS Appl Mater Interfaces* 11(2):2282–2294. <https://doi.org/10.1021/acsam.8b18312>
- [22] Tang Z, Yao D, Du D, Ouyang J (2020) Highly machine-washable e-textiles with high strain sensitivity and high thermal conduction. *Journal of Materials Chemistry C* 8(8):2741–2748. <https://doi.org/10.1039/c9tc06155j>

- [23] Kim SJ, Song W, Yi Y, Min BK, Mondal S, An KS, Choi CG (2018) High durability and waterproofing rgo/swcnt-fabric-based multifunctional sensors for human-motion detection. *ACS Appl Mater Interfaces* 10(4):3921–3928. <https://doi.org/10.1021/acsami.7b15386>
- [24] Liu H, Li Q, Bu Y, Zhang N, Wang C, Pan C, Mi L, Guo Z, Liu C, Shen C (2019) Stretchable conductive nonwoven fabrics with self-cleaning capability for tunable wearable strain sensor. *Nano Energy* 66:104143. <https://doi.org/10.1016/j.nanoen.2019.104143>
- [25] Chun S, Son W, Kim DW, Lee J, Min H, Jung H, Kwon D, Kim AH, Kim YJ, Lim SK, Pang C, Choi C (2019) Water-resistant and skin-adhesive wearable electronics using graphene fabric sensor with octopus-inspired microsuckers. *ACS Appl Mater Interfaces* 11(18):16951–16957. <https://doi.org/10.1021/acsami.9b04206>
- [26] Liu X, Tang C, Du X, Xiong S, Xi S, Liu Y, Shen X, Zheng Q, Wang Z, Wu Y, Horner A, Kim J-K (2017) A highly sensitive graphene woven fabric strain sensor for wearable wireless musical instruments. *Mater Horiz* 4(3):477–486. <https://doi.org/10.1039/c7mh00104e>
- [27] Ren J, Wang C, Zhang X, Carey T, Chen K, Yin Y, Torrisi F (2017) Environmentally-friendly conductive cotton fabric as flexible strain sensor based on hot press reduced graphene oxide. *Carbon* 111:622–630. <https://doi.org/10.1016/j.carbon.2016.10.045>
- [28] Hong X, Peng T, Zhu C, Wan J, Li Y (2021) Electromagnetic shielding, resistance temperature-sensitive behavior, and decoupling of interfacial electricity for reduced graphene oxide paper. *J Alloy Compd* 882:160756. <https://doi.org/10.1016/j.jallcom.2021.160756>
- [29] Liu Y, Xia L, Zhang Q, Guo H, Wang A, Xu W, Wang Y (2019) Structure and properties of carboxymethyl cotton fabric loaded by reduced graphene oxide. *Carbohydr Polym* 214:117–123. <https://doi.org/10.1016/j.carbpol.2019.03.028>
- [30] Cheng H, Dong Z, Hu C, Zhao Y, Hu Y, Qu L, Chen N, Dai L (2013) Textile electrodes woven by carbon nanotube-graphene hybrid fibers for flexible electrochemical capacitors. *Nanoscale* 5(8):3428–3434. <https://doi.org/10.1039/c3nr00320e>
- [31] Balandin AA, Ghosh S, Bao W, Calizo I, Teweldebrhan D, Miao F, Lau CN (2008) Superior thermal conductivity of single-layer graphene. *Nano Lett* 8(3):902–907. <https://doi.org/10.1021/nl0731872>
- [32] Reddy KR, Gandla S, Gupta D (2019) Highly sensitive, rugged, and wearable fabric strain sensor based on graphene clad polyester knitted elastic band for human motion monitoring. *Adv Mater Interfaces* 6(16):1900409. <https://doi.org/10.1002/admi.201900409>
- [33] Liu Y, Zhang D, Wang K, Liu Y, Shang Y (2016) A novel strain sensor based on graphene composite films with layered structure. *Compos A Appl Sci Manuf* 80:95–103. <https://doi.org/10.1016/j.compositesa.2015.10.010>
- [34] Liu H, Li Y, Dai K, Zheng G, Liu C, Shen C, Yan X, Guo J, Guo Z (2016) Electrically conductive thermoplastic elastomer nanocomposites at ultralow graphene loading levels for strain sensor applications. *Journal of Materials Chemistry C* 4(1):157–166. <https://doi.org/10.1039/c5tc02751a>
- [35] Cai G, Yang M, Xu Z, Liu J, Tang B, Wang X (2017) Flexible and wearable strain sensing fabrics. *Chem Eng J* 325:396–403. <https://doi.org/10.1016/j.cej.2017.05.091>
- [36] Shao F, Bian SW, Zhu Q, Guo MX, Liu S, Peng YH (2016) Fabrication of polyaniline/graphene/polyester textile electrode materials for flexible supercapacitors with high capacitance and cycling stability. *Chem Asian J* 11(13):1906–1912. <https://doi.org/10.1002/asia.201600411>
- [37] He S, Xin B, Chen Z, Liu Y (2018) Flexible and highly conductive Ag/G-coated cotton fabric based on graphene dipping and silver magnetron sputtering. *Cellulose* 25(6):3691–3701. <https://doi.org/10.1007/s10570-018-1821-4>
- [38] Niu B, Hua T, Hu H, Xu B, Tian X, Chan K, Chen S (2019) A highly durable textile-based sensor as a human-worn material interface for long-term multiple mechanical deformation sensing. *Journal of Materials Chemistry C* 7(46):14651–14663. <https://doi.org/10.1039/c9tc04006d>
- [39] Hummers WS Jr, Offeman RE (1958) Preparation of graphitic oxide. *J Am Chem Soc* 80(6):1339
- [40] Hong X, Yu W, Wang A, Chung D (2016) Graphite oxide paper as a polarizable electrical conductor in the through-thickness direction. *Carbon* 109:874–882
- [41] Park TH, Yu S, Koo M, Kim H, Kim EH, Park JE, Ok B, Kim B, Noh SH, Park C, Kim E, Koo CM, Park C (2019) Shape-Adaptable 2D Titanium Carbide (MXene) Heater. *ACS Nano* 13(6):6835–6844. <https://doi.org/10.1021/acs.nano.9b01602>
- [42] Jeong HK, Yun PL, Lahaye RJWE, Park MH, Kay HA, Ick JK, Yang CW, Chong YP, Ruoff RS, Young HL (2008) Evidence of graphitic AB stacking order of graphite oxides. *J Am Chem Soc* 130(4):1362–1366. <https://doi.org/10.1021/ja076473o>
- [43] Zhou X, Shi T, Wu J, Zhou H (2013) (001) Facet-exposed anatase-phase TiO<sub>2</sub> nanotube hybrid reduced graphene oxide composite: Synthesis, characterization and application in photocatalytic degradation. *Appl Surf Sci* 287:359–368. <https://doi.org/10.1016/j.apsusc.2013.09.156>
- [44] Mecozzi M, Nisini L (2019) The differentiation of biodegradable and non-biodegradable polyethylene terephthalate (PET) samples by FTIR spectroscopy: A potential



- support for the structural differentiation of PET in environmental analysis. *Infrared Phys Technol* 101:119–126. <https://doi.org/10.1016/j.infrared.2019.06.008>
- [45] Razavizadeh M, Jamshidi M (2016) Adhesion of nitrile rubber (NBR) to polyethylene terephthalate (PET) fabric. Part 1: PET surface modification by methylenediphenyl diisocyanate (MDI). *Appl Surf Sci* 360:429–435. <https://doi.org/10.1016/j.apsusc.2015.10.137>
- [46] Fuente E, Menéndez JA, Díez MA, Suárez D, Montes-Morán MA (2003) Infrared spectroscopy of carbon materials: A quantum chemical study of model compounds. *J Phys Chem B* 107(26):6350–6359
- [47] Xu L-L, Guo M-X, Liu S, Bian S-W (2015) Graphene/cotton composite fabrics as flexible electrode materials for electrochemical capacitors. *RSC Adv* 5(32):25244–25249. <https://doi.org/10.1039/c4ra16063k>
- [48] Szabó T, Berkesi O, Forgó P, Josepovits K, Sanakis Y, Petridis D, Dékány I (2006) Evolution of surface functional groups in a series of progressively oxidized graphite oxides. *Chem Mater* 18(11):2740–2749. <https://doi.org/10.1021/cm060258+>
- [49] Babaahmadi V, Montazer M (2016) Reduced graphene oxide/SnO<sub>2</sub> nanocomposite on PET surface: Synthesis, characterization and application as an electro-conductive and ultraviolet blocking textile. *Colloids Surf, A* 506:507–513. <https://doi.org/10.1016/j.colsurfa.2016.07.025>
- [50] Tian M, Hu X, Qu L, Zhu S, Sun Y, Han G (2016) Versatile and ductile cotton fabric achieved via layer-by-layer self-assembly by consecutive adsorption of graphene doped PEDOT: PSS and chitosan. *Carbon* 96:1166–1174. <https://doi.org/10.1016/j.carbon.2015.10.080>
- [51] Seyedin S, Razal JM, Innis PC, Jeiranikhameneh A, Beirne S, Wallace GG (2015) Knitted strain sensor textiles of highly conductive all-polymeric fibers. *ACS Appl Mater Interfaces* 7(38):21150–21158. <https://doi.org/10.1021/acsami.5b04892>

**Publisher's Note** Springer Nature remains neutral with regard to jurisdictional claims in published maps and institutional affiliations.